Few-cycle laser wakefield acceleration on solid targets with controlled plasma scale length

N. Zaïm,[1, a)] F. Böhle,[1] M. Bocoum,[1] A. Vernier,[1] S. Haessler,[1] X. Davoine,[2] L. Videau,[2] J. Faure,[1] R. Lopez-Martens[1]

[1)] *LOA, ENSTA ParisTech, CNRS, Ecole polytechnique, Université Paris-Saclay, Palaiseau, France*

[2)] *CEA, DAM, DIF, F-91297 Arpajon, France*

(Dated: 17 January 2019)

We measure the emission of energetic electrons from the interaction between relativistic-intensity ultrashort laser pulses and a solid density plasma with tunable density gradient scale length. We detect an electron beam that only appears with few-cycle pulses ($<$ 10 fs) and large plasma scale lengths ($L > \lambda_0$). Numerical simulations, in agreement with the experiments, reveal that these electrons are accelerated by a laser wakefield. Plasma waves are indeed resonantly excited by the few-cycle laser pulses in the near-critical density region of the plasma. Electrons are then injected by ionization into the plasma waves and accelerated to relativistic energies. In this laser wakefield acceleration regime, the plasma waves are rotated by the plasma density gradient which results in the electrons not being emitted in the same direction as the driving laser pulse.

I. INTRODUCTION

Since the recent advent of ultrahigh intensity lasers, bright particle and radiation sources with femtosecond duration have been developed from relativistic laser-plasma interactions. These new sources are expected to find applications in various fields including medicine, imaging and ultrafast probing of matter[1,2]. Laser wakefield acceleration (LWFA) is an efficient process for driving relativistic electron beams with few femtosecond durations[3] and energies in the 100 MeV to multi-GeV range[4–6], or more recently in the few-MeV range with kHz lasers[7–9]. In this scheme, the laser pulse ponderomotive force drives a high amplitude plasma wave that is able to trap and accelerate electrons over very short distances[10]. Usually, LWFA takes place in mm-scale underdense plasmas (gas jets) but is quite inefficient with solid targets. Indeed, for solid-density plasmas, the processes responsible for transferring the laser energy to particles and radiation are radically different. Understanding the pathways and mechanisms of energy transfer to the plasma electrons is a complex and fundamental question that has implications for ion acceleration[11] and high harmonic generation[12].

It is well known that the plasma density profile at the front surface is a key parameter that can dramatically transform the nature of the interaction[13–18]. When the plasma scale length is short compared to the laser wavelength ($L < \lambda_0/10$), the physics is now fairly well understood. At moderate intensity, vacuum heating[19] is the dominant mechanism for energy transfer to the electrons. At relativistic intensities, the physics becomes more complex: the laser field triggers a periodic push-pull motion of the front surface that follows the sign of the laser field[20,21]. This nonlinear periodic motion leads to high harmonic generation via the relativistic oscillating mirror mechanism[22,23] and also results in electron ejection from the front surface[21,24,25]. These electrons are subsequently injected into the reflected laser field where they can directly gain large amounts of energy[24]. In this regime, electron emission has been reported to be optimal when the gradient scale length is on the order of $\sim \lambda_0/10$, with electron energies ranging from 100 keV to multi-MeV, depending on laser intensity[24–29].

For longer gradient scale lengths, interaction in the near-critical density part of the plasma, which has also been investigated in the context of ion acceleration[30–33], becomes significant. The physics gets extremely complex and there is no unified description of energy transfer and electron acceleration. There is a wide disparity of experimental results and various mechanisms have been proposed, including resonant absorption[34,35], J$\times$B heating[36], ponderomotive acceleration[37], stochastic heating[38,39], acceleration by surface quasistatic fields[40] or direct laser acceleration[41,42]. However, it is still unclear what mechanisms actually arise in experiments and the precise experimental conditions under which they appear are not known. This may be due to the lack of control and measurement of the density gradients, which makes the interpretations difficult. In this article, we show that by using few-cycle laser pulses with durations as short as 3.5 fs, we find a regime where LWFA occurs in the near-critical density region of the plasma. Even though this mechanism was previously suggested to explain experimental results with thick solid targets[35,43], LWFA is here clearly identified by varying and precisely controlling the key parameters of the interaction, namely the gradient length and the pulse duration, and by performing PIC simulations with realistic plasma density profiles. We find that this regime, which results in the emission of a $\approx 25^\circ$-wide stable electron beam, only occurs with few-cycle laser pulses.

II. EXPERIMENTAL SETUP AND RESULTS

The experiments are performed with the Salle Noire laser system at the Laboratoire d'Optique Appliquée (LOA). The laser delivers 2.6-mJ pulses at 1-kHz repetition rate with an extremely high temporal contrast ($> 10^{10}$)[44]. The 800 nm,

[a)] Electronic mail: neil.zaim@ensta-paristech.fr

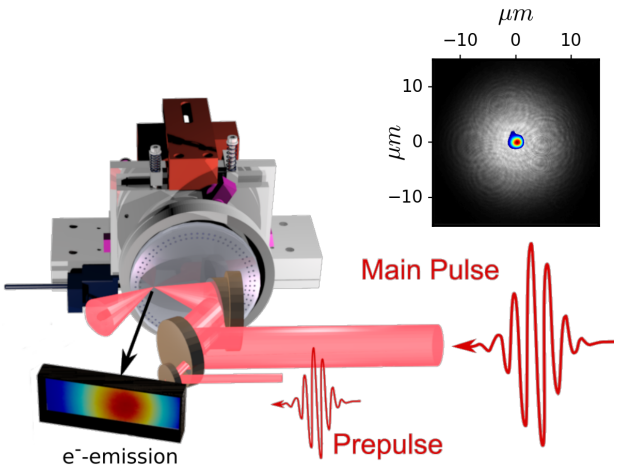

FIG. 1. Schematic of the experimental setup. The laser pulses interact at 1-kHz repetition rate with a fused silica rotating target. Inset: superimposition of the on-target prepulse (white) and main pulse (color) focal spots.

24 fs laser pulses are post-compressed in a helium-filled stretched hollow-core fiber[45,46]. The pulse duration can be tuned by changing the pressure in the fiber, thereby providing near Fourier transform limited pulses from 3.5 fs to 24 fs. The laser beam is focused down to a 1.75 μm FWHM spot resulting in peak intensities ranging from $2.3\times10^{18}\,\mathrm{W/cm^2}$ ($a_0\simeq1$) for 24 fs pulses to $1.6\times10^{19}\,\mathrm{W/cm^2}$ ($a_0\simeq2.7$) for 3.5 fs pulses. Here, a_0 is defined as the normalized amplitude of the peak laser field: $a_0=E_{\mathrm{MAX}}/E_0$ with $E_0=m_e c\omega_0/e$ where ω_0 is the laser frequency, c is the speed of light in vacuum and m_e and e are the electron mass and charge respectively. In this experiment, represented in Fig. 1, p-polarized pulses impinge on an optically flat fused silica (SiO_2) target with an incidence angle $\theta_i=55^\circ$. A spatially overlapped prepulse, created by picking off $\approx4\%$ of the main pulse through a holey mirror, is focused to a much larger 13 μm FWHM spot (see inset of Fig. 1) in order to generate a transversely homogeneous plasma that expands into vacuum. The plasma density profile during the interaction is controlled by varying the delay, Δt, between the prepulse and the main pulse. The density scale length is estimated experimentally using spatial domain interferometry and assuming isothermal expansion[47]. Backward electron emission is measured using a Lanex screen, protected by a 13 μm thick Al-foil, which detects electrons with energies >150 keV. The Lanex screen was calibrated prior to the experiment using a 3-MeV RF accelerator. The absolute charge is estimated from the electron energy spectrum obtained from the PIC simulations described below, combined with the known spectral response of the Lanex screen. The resulting uncertainty, of the order of 50%, is mainly due to the fact that the exact shape of the energy spectra was not measured. The angular electron distribution in the backward direction is recorded for $-3^\circ<\theta<75^\circ$ and $-15^\circ<\phi<15^\circ$ where θ and ϕ are the angles with respect to target normal respectively in the incidence and transverse planes.

Figures 2(a)-2(f) show the measured electron signal as a function of the delay between the prepulse and the main pulse for 5 different laser pulse durations. We first find a strong electron emission for short delays ($\Delta t<20$ ps), corresponding to a sharp plasma-vacuum interface. This emission, detected for every pulse duration, is optimal for a delay $\Delta t\approx9$ ps, i.e. $L<\lambda_0/5$. In this regime, the push-pull mechanism mentioned in the introduction is responsible for the ejection of electrons from the plasma[21,24,29]. A typical electron angular distribution in this case is displayed in Fig. 2(g), showing a broad divergence angle of $\approx50^\circ$.

As the delay is further increased, the detected charge drops (10 ps $<\Delta t<30$ ps), and then rises again for longer delays ($\Delta t>50$ ps). This time however, electrons are only emitted when few-cycle pulses ($\leq$10 fs) are used. Note that chirping a few-cycle pulse to increase its duration results in a similar decline of the electron signal, as can be seen in Fig. 3. This is thus a very distinct physical regime, in which the gradient length is much larger ($L>\lambda_0$) and the duration of the laser pulse plays a major role. In this case, the obtained electron beams have more charge and a narrower divergence angle of $\approx25^\circ$ as is visible in Fig. 2(h). The electrons are emitted near the specular direction, with a slight shift towards the normal direction. The detected signal is very stable over a wide range of delays (50 ps$<\Delta t<$200 ps), indicating that the electron ejection mechanism is not highly sensitive to the exact shape of the plasma density profile. Contrary to the emission of electrons for short delays ($\Delta t<20$ ps) which is strongly correlated with high-harmonics generation[25], we measure no significant high-harmonics signal at these longer delays ($\Delta t>30$ ps).

III. PIC SIMULATIONS

To understand the origin of this new electron emission process, we turn to 2D Particle-In-Cell (PIC) simulations using the code WARP[48,49] coupled to the high performance PICSAR library[50–53]. We use the same laser parameters as in the experiments (more details are given in the Supplementary Material). A moving window is started after the interaction in order to follow the accelerated electrons far from the plasma. We took great care in providing a realistic description of the plasma density gradient. First, the plasma is initially partially ionized (up to Si^{4+} and O^{2+}) in order to model ionization by the prepulse. The initial ionization states are estimated from the prepulse peak intensity ($\sim10^{15}\,\mathrm{W/cm^2}$) and the intensity thresholds for barrier-suppression ionization[54] in silicon and oxygen. Further ionization by the main pulse is also taken into account in the simulations. Second, the plasma density profile is obtained by performing hydrodynamic 1D simulations with the code ESTHER[55]. Figure 4 shows the resulting profiles for 4 different values of the delay between the prepulse and the main pulse. Note that the density profiles are not always exponential in Fig. 4, contrary to results from models assuming isothermal expansion. The gradient appears to have an exponential shape only for short delays (i.e. for sharp plasma-vacuum interfaces) but not for longer delays. The isothermal

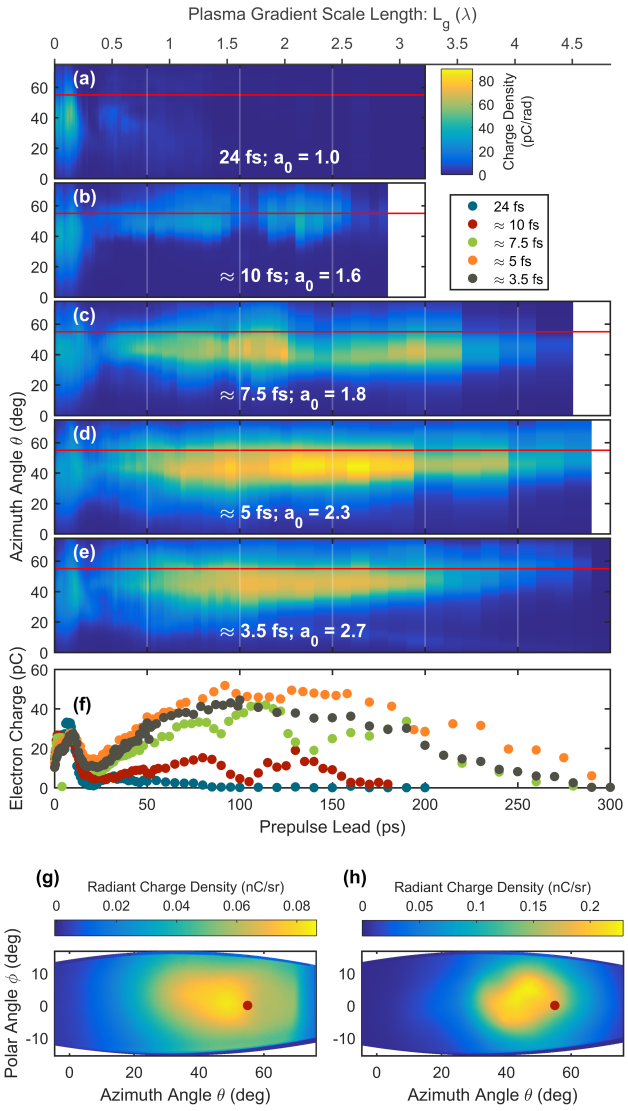

FIG. 2. (a)-(e) Electron angular distribution integrated over the ϕ angle as a function of the delay between the prepulse and the main pulse for respective pulse durations of 24, 10, 7.5, 5 and 3.5 fs. (f) Total ejected charge as a function of the delay between prepulse and main pulse. (g), (h) Typical electron angular distribution obtained with 5-fs pulses respectively in the short ($\Delta t = 9$ ps) and long ($\Delta t = 140$ ps) plasma scale length regimes. The gradient scale lengths given in the top axis are obtained from interferometric measurements[47]. The white lines in (a)-(e) represent the prepulse leads corresponding to the ticks in (f). The red lines and dots mark the specular direction.

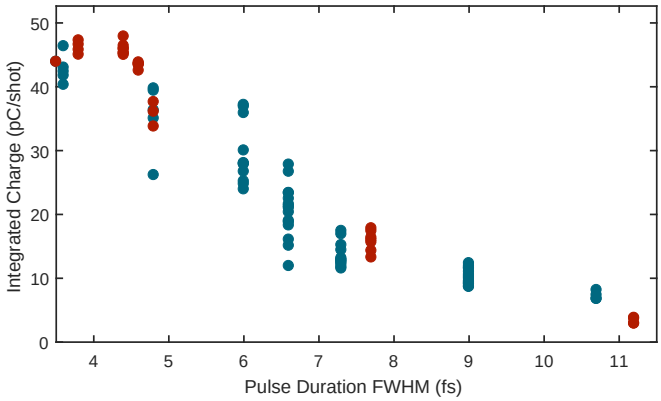

FIG. 3. Total detected charge as a function of pulse duration for a delay $\Delta t = 90$ ps between the prepulse and the main pulse. The pulse duration is tuned here by chirping positively (red points) or negatively (blue points) the 3.5-fs driving laser.

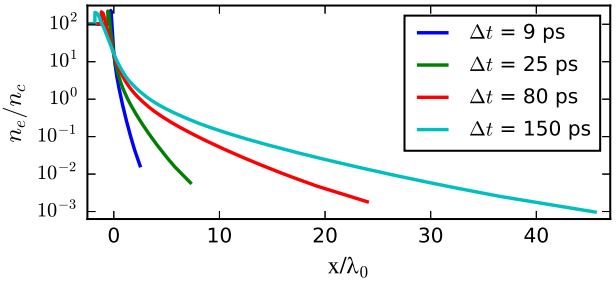

FIG. 4. Results from 1D hydrodynamic simulations. Normalized electron density n_e/n_c as a function of position x for different delays after a prepulse with fluence $50\,\mathrm{J/cm^2}$ ionizes a solid fused-silica target. $x = 0$ is the initial solid-vacuum interface position. $n_c = m_e\varepsilon_0\omega_0^2/e^2$ is the critical density above which the laser cannot propagate. ε_0 is the vacuum permittivity.

hypothesis, used to estimate the gradient scale length in the previously mentioned interferometric measurements[47], likely fails due to radiation and convection losses on these longer timescales. In our case, the electron beam appears for long delays Δt and we therefore use the density profiles shown in Fig. 4 as inputs for the PIC simulations.

Snapshots from two different PIC simulations are shown in Fig. 5. Both simulations use the plasma density profile obtained with a delay Δt = 80 ps (i.e. the red curve in Fig. 4), a value for which the electron beam is detected in the experiments. The pulse duration is either 5 fs or 24 fs, resulting in peak intensities of $10^{19}\,\mathrm{W/cm^2}$ ($a_0 = 2.15$) and $2.1\times10^{18}\,\mathrm{W/cm^2}$ ($a_0 = 0.98$) respectively.

The first striking feature is the formation of high amplitude plasma waves in the wake of the 5-fs pulse. Their wavefront is bent by the density gradient, akin to the plasma waves generated by Brunel electrons in the coherent wake emission mechanism of high-harmonic generation[12]. Even though these wakefields appear in the whole region where the 5-fs pulse propagates, inside which the density ranges from $n_c/1000$ to $n_c\cos^2\theta_i \sim 0.3n_c$[56], they are completely absent in the 24-fs pulse simulation. This can be easily explained by the fact that wakefield excitation is optimal at the resonance condition, i.e. when the pulse duration is on the order of half the plasma wavelength[10]: $\tau \simeq \lambda_p/2c$. This gives a resonant density of $n_c/14$ for 5-fs pulses, versus $n_c/300$ for 24-fs pulses, explaining why large wakefields appear for the few-cycle pulse only (see also Supplementary Material).

Some electrons, represented in green in Fig. 5, are trapped and accelerated by the plasma waves' strong electric fields, that reach up to 1 TV/m. The angular and energy distribu-

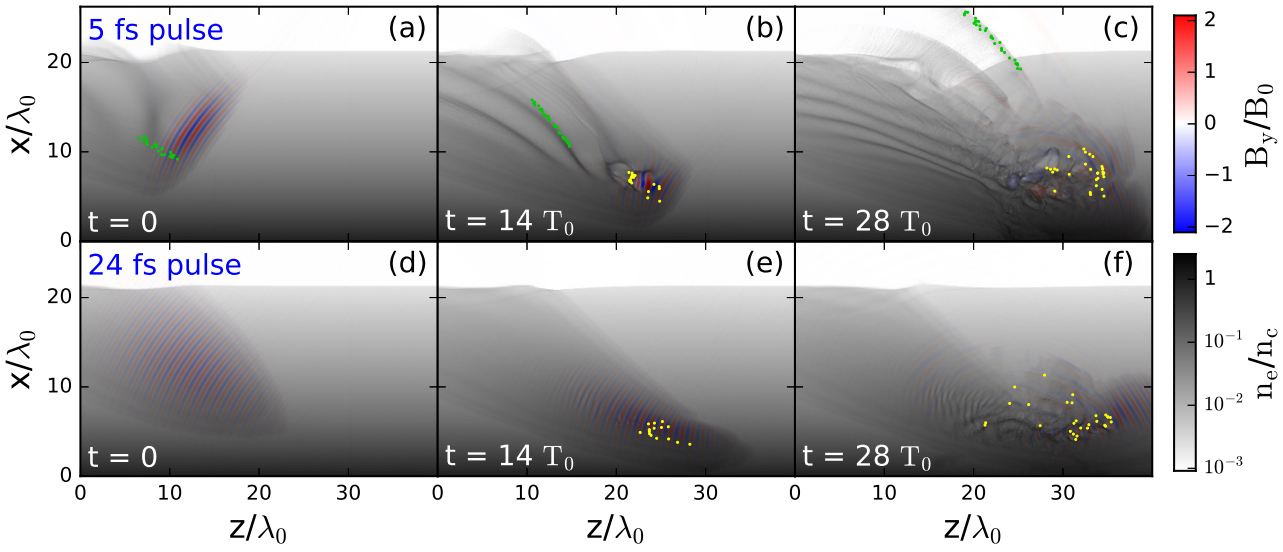

FIG. 5. Laser magnetic field and electron density from PIC simulations with a large plasma scale length (Δt = 80 ps) and a pulse duration of (a)-(c) 5 fs or (d)-(f) 24 fs. The green and yellow dots show a sample of ejected electrons. T_0 is the laser optical oscillation period and $B_0 = E_0/c$ with E_0 defined earlier. See also videos for a more comprehensive view of the simulations.

tion of these LWFA electrons is shown in the green curves of Fig. 6(a) and Fig. 6(c) respectively. Their energy spectrum extends to $\approx$ 2.5 MeV and their total ejected charge is $\approx$ 7 pC/μm. These electrons are emitted in the same direction as the electrons detected at long delays in experiments (see the red curve in Fig. 6(a)). Moreover, as in experiments, these electrons only appear for few-cycle pulses. We therefore conclude that the electron beam detected at long delays in experiments originates from LWFA. We may notice that the angular distribution of these electrons is significantly narrower in the simulation than in experiments. This is likely due to space charge effects during the propagation of the electron beam to the detector, which we expect to be important for a sub-MeV beam with tens of pC of charge. The electrons are indeed only propagated for tens of microns in the simulation while the Lanex screen is located $\approx$ 10 cm away from the target in experiments.

In the simulations, the LWFA electrons come from the L-shell of silicon. They have high binding energies (from $\approx$ 150 eV to $\approx$ 500 eV) and can therefore only be ionized by the huge electric fields inside the main laser pulse. The fact that only electrons ionized in the center of the pulse are accelerated suggests that injection by ionization, a well-known mechanism in underdense plasmas[57,58], is responsible for trapping the electrons into the wakefields. Taking field ionization into account is therefore needed to properly describe the injection of electrons into the plasma waves and more generally to correctly model laser interactions with overdense plasmas when the plasma scale length is large.

Another family of electrons, shown in yellow in Fig. 5 and labelled "reflection electrons", is ejected from the plasma in the simulations. These electrons are accelerated at the reflection point of the laser, where the density is $n_c \cos^2\theta_i$. Their angular and energy distributions are displayed in the yellow

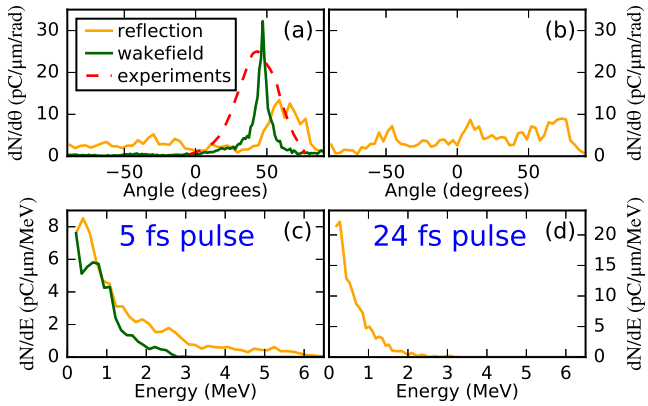

FIG. 6. (a),(b) Angular and (c),(d) energy distribution of the two families of electrons that are ejected in the (a),(c) 5 fs and (b),(d) 24 fs simulation. The distributions are obtained at the end of the simulation, long after the interaction. The red dashed curve in (a) shows for comparison the experimental angular distribution integrated along the ϕ angle obtained with a 5 fs pulse and an 80 ps prepulse lead, in arbitrary units.

curves of Fig. 6. This family of electrons, which appears for both 5-fs and 24-fs pulses and has a very large angular divergence spreading across all directions, is not detected in experiments. This fact shows that our 2D PIC simulations do not accurately reproduce the ratio between the two populations. This second family of electrons would likely be attenuated in more accurate but more costly 3D simulations. However, this is not a major concern because the simulations explain the main experimental observations, i.e. a well-defined beam of LWFA electrons that appears only for extremely short pulse duration.

It is also worth noting that the same qualitative results are found when the simulations are performed with an exponential density profile with $L = 3\lambda_0$, thus confirming our previous observation that the electron ejection mechanism is not highly sensitive to the exact shape of the plasma density profile. Another interesting point is that a similar trend can be found when the intensities are interchanged in the simulations (i.e. when the 5-fs simulation is carried out with a peak intensity of $2.1 \times 10^{18}\,\mathrm{W/cm^2}$, while the 24-fs simulation is performed with a $1 \times 10^{19}\,\mathrm{W/cm^2}$ peak intensity). In this case, even though the laser pulse energy is 25 times lower in the 5-fs simulation, a very small number of electrons remain laser wakefield accelerated while there is still no plasma wave formation in the 24-fs simulation (see Supplementary Material). These simulations show a clear effect of pulse duration and confirm that the emergence of the electron beam is not simply due to the increase in intensity when reducing the pulse duration.

IV. PLASMA WAVE FORMATION AND ELECTRON ACCELERATION IN A TRANSVERSE GRADIENT

A unique feature of this acceleration regime is that the electrons are not emitted in the same direction as the driving laser pulse, as is usually the case with LWFA, even with similar laser parameters and plasma densities[7,8]. This is because the wakefields' wavefronts are rotated by the density gradient. To explain this rotation, we use a simple heuristic model based on the following assumptions: (i) the plasma wave is initiated at the temporal center of the laser pulse. This is formally equivalent to an infinitely short driving pulse and is reasonable if the pulse duration is much shorter than a plasma period. (ii) The plasma wave is longitudinal, i.e. the electrons forming it oscillate in the direction of laser propagation. This assumption is equivalent to an infinitely wide (1D) driving laser pulse and is valid when the laser transverse size is larger than a plasma wavelength. (iii) The center of the laser pulse travels at c, neglecting the decrease in group velocity. (iv) The phase of the plasma wave varies at each point at the local plasma frequency. This is valid if the gradient scale length is much larger than the plasma wavelength[12]. With these assumptions, the phase φ of the plasma wave is:

$$\varphi(x,z,t) = \omega_p(x)(t - t_0(x,z)) \tag{1}$$

Here, ω_p is the local plasma frequency and $t_0 = (z\sin\theta_i - x\cos\theta_i)/c$ is the time at which the temporal center of the laser pulse excites the plasma wave. Plasma wavefronts obtained using Eq. (1) in an exponential density gradient are shown in Fig. 7. Even though this simple model is not perfectly valid for the considered experimental case, it can qualitatively reproduce the shape of the plasma waves. Physically, the rotation of the wavefronts can be explained by the transverse density gradient seen by the laser, i.e. the fact that one side of the laser pulse excites a plasma wave with a higher frequency than the other. A given phase will therefore be reached quicker in the region of higher frequency, which results in rotated wavefronts.

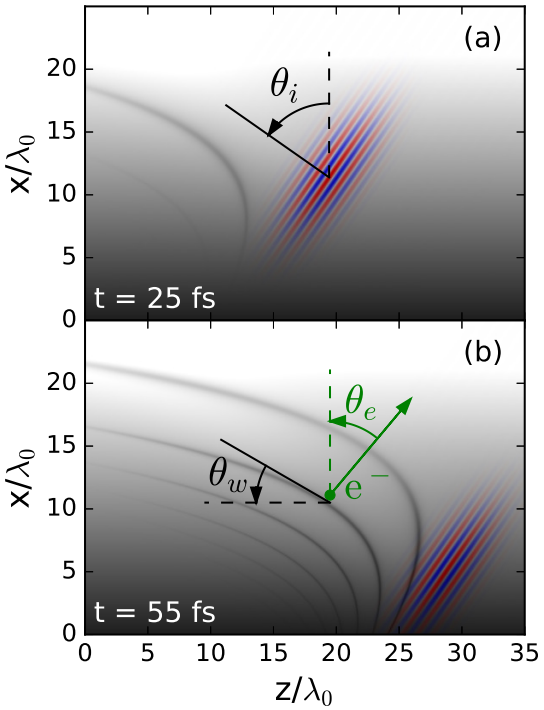

FIG. 7. Wavefronts (darker lines) obtained using Eq. (1) during the propagation of a laser pulse (represented in blue and red) in a plasma with an exponential density profile ($L = 3\lambda_0$). Two consecutive wavefronts are separated by a phase of 2π.

We can also use this model to qualitatively explain the measured angular distribution. Let us consider an electron moving with an angle θ_e with respect to the x-axis at a position where the wavefront of the plasma wave makes an angle θ_w with respect to the z-axis (see Fig. 7(b)). We first note that since the plasma frequency only depends on x, the phase velocity of the plasma waves in the z-direction is $(v_\varphi)_z = c/\sin\theta_i$. We can then, using the law of sines, calculate the phase velocity along the direction of electron motion:

$$(v_\varphi)_{\theta_e} = \frac{\sin\theta_w}{\cos(\theta_e - \theta_w)\sin\theta_i}c \tag{2}$$

If the electron is trapped in the wakefield, its velocity is mainly colinear with the electric field of the plasma waves, i.e. perpendicular to the wavefronts. In this case, we have $\theta_e \approx \theta_w$ and Eq. (2) is simplified to:

$$(v_\varphi)_{\theta_e} = \frac{\sin\theta_e}{\sin\theta_i}c \tag{3}$$

Trapping of electrons by the plasma wave is only possible if the phase velocity of the wakefield is lower than c, meaning in our case that electrons can only be emitted when $\theta_e < \theta_i$. Furthermore, electron acceleration to relativistic energies is

efficient when the phase velocity is close to c. Equation (3) therefore indicates that the electrons should be emitted close to the specular direction with a slight shift towards the normal direction, in good agreement with experiments and simulations. Electrons directed closer to the grazing direction ($\theta_e > \theta_i$) cannot be trapped as the phase velocity of the plasma waves in their direction is greater than c while electrons emitted close to the normal direction cannot reach high energies as they would quickly dephase from the plasma waves.

V. CONCLUSION

In conclusion, we detect an electron beam that only appears for few-cycle pulses and large plasma scale lengths. Particle-In-Cell simulations successfully explain the experimental results: the detected electrons are injected by ionization into wakefields formed behind the pulse. These plasma waves can only be efficiently excited by few-cycle pulses at these near-critical densities, explaining why this new electron emission mechanism is only observed with extremely short pulses. A singular trait of this acceleration regime is that, due to the rotation of the wakefields induced by the density gradient, the electron beam is not emitted in the same direction as the driving laser pulse. This work offers a better understanding of the interaction between ultraintense laser pulses and solid targets and confirms that extremely short pulse durations and controlled plasma conditions provide access to new acceleration regimes.

VI. SUPPLEMENTARY MATERIAL

Supplementary material consists of 6 sections. In the first section, we present the experimental results obtained when reducing the main laser pulse intensity. In the second section, we provide detailed explanations regarding how few-cycle laser pulses are modeled in our Particle-In-Cell simulations. In the third section, we give more informations concerning the numerical parameters of the Particle-In-Cell simulations presented in the main text. In the fourth section, we present simulations performed with the other pulse durations studied experimentally. In the fifth section, we present more exhaustively the simulations with interchanged intensities that are mentioned in the main text. In the sixth section, we estimate the amplitude of the plasma waves generated in our experiments using the 1D nonlinear theory of wakefield generation.

VII. ACKNOWLEDGMENTS

We would like to thank H. Vincenti for his help and expertise with PIC simulations and for insightful discussions. This work was funded by the European Research Council under Contract No. 306708 (ERC Starting Grant No. FEMTOELEC), the Région Île-de-France (under Contract No. SESAME-2012- ATTOLITE), the Agence Nationale pour la Recherche (under Contracts No. ANR-11-EQPX-005-ATTOLAB and No. ANR-14-CE32-0011-03), the Extreme Light Infrastructure-Hungary Non-Profit Ltd (under Contract No. NLO3.6LOA) and the LabEx PALM (ANR-10-LABX-0039). This work was granted access to the HPC resources of CINES under the allocation A0020506057 made by GENCI.

[1] V. Malka, J. Faure, Y. A. Gauduel, E. Lefebvre, A. Rousse, and K. Ta Phuoc, "Principles and applications of compact laser–plasma accelerators," Nature Physics **44**, 447–453 (2008).

[2] F. Albert and A. G. R. Thomas, "Applications of laser wakefield accelerator-based light sources," Plasma Physics and Controlled Fusion **58**, 103001 (2016).

[3] O. Lundh, J. Lim, C. Rechatin, L. Ammoura, A. Ben-Ismail, X. Davoine, G. Gallot, J.-P. Goddet, E. Lefebvre, V. Malka, and J. Faure, "Few femtosecond, few kiloampere electron bunch produced by a laser-plasma accelerator," Nat. Phys. **7**, 219 (2011).

[4] J. Faure, Y. Glinec, A. Pukhov, S. Kiselev, S. Gordienko, E. Lefebvre, J.-P. Rousseau, F. Burgy, and V. Malka, "A laser-plasma accelerator producing monoenergetic electron beams," Nature **431**, 541–544 (2004).

[5] X. Wang, R. Zgadzaj, N. Fazel, Z. Li, S. A. Yi, X. Zhang, W. Henderson, Y. Y. Chang, R. Korzekwa, H. E. Tsai, C. H. Pai, H. Quevedo, G. Dyer, E. Gaul, M. Martinez, A. C. Bernstein, T. Borger, M. Spinks, M. Donovan, V. Khudik, G. Shvets, T. Ditmire, and M. C. Downer, "Quasi-monoenergetic laser-plasma acceleration of electrons to 2 GeV," Nat. Comm. **4** (2013).

[6] W. P. Leemans, A. J. Gonsalves, H.-S. Mao, K. Nakamura, C. Benedetti, C. B. Schroeder, C. Tóth, J. Daniels, D. E. Mittelberger, S. S. Bulanov, J.-L. Vay, C. G. R. Geddes, and E. Esarey, "Multi-GeV electron beams from capillary-discharge-guided subpetawatt laser pulses in the self-trapping regime," Phys. Rev. Lett. **113**, 245002 (2014).

[7] D. Guénot, D. Gustas, A. Vernier, B. Beaurepaire, F. Böhle, M. Bocoum, M. Lozano, A. Jullien, R. Lopez-Martens, A. Lifschitz, and J. Faure, "Relativistic electron beams driven by khz single-cycle light pulses," Nat. Photon. **11**, 293–296 (2017), letter.

[8] D. Gustas, D. Guénot, A. Vernier, S. Dutt, F. Böhle, R. Lopez-Martens, A. Lifschitz, and J. Faure, "High-charge relativistic electron bunches from a khz laser-plasma accelerator," Phys. Rev. Accel. Beams **21**, 013401 (2018).

[9] F. Salehi, A. J. Goers, G. A. Hine, L. Feder, D. Kuk, B. Miao, D. Woodbury, K. Y. Kim, and H. M. Milchberg, "Mev electron acceleration at 1khz with $<$ 10mj laser pulses," Opt. Lett. **42**, 215–218 (2017).

[10] E. Esarey, C. B. Schroeder, and W. P. Leemans, "Physics of laser-driven plasma-based electron accelerators," Rev. Mod. Phys. **81**, 1229–1285 (2009).

[11] A. Macchi, M. Borghesi, and M. Passoni, "Ion acceleration by superintense laser-plasma interaction," Rev. Mod. Phys. **85**, 751–793 (2013).

[12] C. Thaury and F. Quéré, "High-order harmonic and attosecond pulse generation on plasma mirrors: basic mechanisms," Journal of Physics B: Atomic, Molecular and Optical Physics **43**, 213001 (2010).

[13] S. C. Wilks and W. L. Kruer, "Absorption of ultrashort, ultra-intense laser light by solids and overdense plasmas," IEEE J. Quant. Electron. **33**, 1954–1968 (1997).

[14] Y. Sentoku, V. Bychenkov, K. Flippo, A. Maksimchuk, K. Mima, G. Mourou, Z. Sheng, and D. Umstadter, "High-energy ion generation in interaction. of short laser pulse with high-density plasma," Applied Physics B **74**, 207–215 (2002).

[15] P. McKenna, D. Carroll, O. Lundh, F. Nürnberg, K. Markey, S. Bandyopadhyay, D. Batani, R. Evans, R. Jafer, S. Kar, and et al., "Effects of front surface plasma expansion on proton acceleration in ultraintense laser irradiation of foil targets," Laser and Particle Beams **26**, 591–596 (2008).

[16] A. J. Kemp, Y. Sentoku, and M. Tabak, "Hot-electron energy coupling in ultraintense laser-matter interaction," Phys. Rev. E **79**, 066406 (2009).

[17] S. Kahaly, S. Monchocé, H. Vincenti, T. Dzelzainis, B. Dromey, M. Zepf, P. Martin, and F. Quéré, "Direct observation of density-gradient effects in harmonic generation from plasma mirrors," Phys. Rev. Lett. **110**, 175001 (2013).

[18] G. G. Scott, V. Bagnoud, C. Brabetz, R. J. Clarke, J. S. Green, R. I. Heathcote, H. W. Powell, B. Zielbauer, T. D. Arber, P. McKenna, and D. Neely,

"Optimization of plasma mirror reflectivity and optical quality using double laser pulses," New Journal of Physics **17**, 033027 (2015).
[19]F. Brunel, "Not-so-resonant, resonant absorption," Phys. Rev. Lett. **59**, 52–55 (1987).
[20]A. A. Gonoskov, A. V. Korzhimanov, A. V. Kim, M. Marklund, and A. M. Sergeev, "Ultrarelativistic nanoplasmonics as a route towards extreme-intensity attosecond pulses," Physical Review E **84**, 046403 (2011).
[21]M. Thévenet, H. Vincenti, and J. Faure, "On the physics of electron ejection from laser-irradiated overdense plasmas," Phys. Plasmas **23**, 063119 (2016).
[22]R. Lichters, J. Meyer-ter Vehn, and A. Pukhov, "Short-pulse laser harmonics from oscillating plasma surfaces driven at relativistic intensity," Physics of Plasmas **3**, 3425–3437 (1996).
[23]T. Baeva, S. Gordienko, and A. Pukhov, "Theory of high-order harmonic generation in relativistic laser interaction with overdense plasma," Phys. Rev. E **74**, 046404 (2006).
[24]M. Thévenet, A. Leblanc, S. Kahaly, H. Vincenti, A. Vernier, F. Quéré, and J. Faure, "Few femtosecond, few kiloampere electron bunch produced by a laser-plasma accelerator," Nat. Phys. **12**, 355 (2015).
[25]L. Chopineau et al. (unpublished).
[26]S. Bastiani, A. Rousse, C. Q. J.-P. Geindre, P. Audebert, G. Harmoniaux, A. Antonetti, and J.-C. Gauthier, "Experimental study of the interaction of subpicosecond laser pulses with solid targets of varying initial scalelengths," Phys. Rev. E **56**, 7179–7185 (1997).
[27]A. G. Mordovanakis, J. Easter, N. Naumova, K. Popov, P.-E. Masson-Laborde, B. Hou, I. Sokolov, G. Mourou, I. V. Glazyrin, W. Rozmus, V. Bychenkov, J. Nees, and K. Krushelnick, "Quasimonoenergetic electron beams with relativistic energies and ultrashort duration from laser-solid interactions at 0.5 khz," Phys. Rev. Lett. **103**, 235001 (2009).
[28]Y. Tian, J. Liu, W. Wang, C. Wang, A. Deng, C. Xia, W. Li, L. Cao, H. Lu, H. Zhang, Y. Xu, Y. Leng, R. Li, and Z. Xu, "Electron emission at locked phases from the laser-driven surface plasma wave," Phys. Rev. Lett. **109**, 115002 (2012).
[29]M. Bocoum, M. Thévenet, F. Böhle, B. Beaurepaire, A. Vernier, A. Jullien, J. Faure, and R. Lopez-Martens, "Anticorrelated emission of high harmonics and fast electron beams from plasma mirrors," Phys. Rev. Lett. **116**, 185001 (2016).
[30]A. Yogo, H. Daido, S. V. Bulanov, K. Nemoto, Y. Oishi, T. Nayuki, T. Fujii, K. Ogura, S. Orimo, A. Sagisaka, J.-L. Ma, T. Z. Esirkepov, M. Mori, M. Nishiuchi, A. S. Pirozhkov, S. Nakamura, A. Noda, H. Nagatomo, T. Kimura, and T. Tajima, "Laser ion acceleration via control of the near-critical density target," Phys. Rev. E **77**, 016401 (2008).
[31]A. Henig, D. Kiefer, K. Markey, D. C. Gautier, K. A. Flippo, S. Letzring, R. P. Johnson, T. Shimada, L. Yin, B. J. Albright, K. J. Bowers, J. C. Fernández, S. G. Rykovanov, H.-C. Wu, M. Zepf, D. Jung, V. K. Liechtenstein, J. Schreiber, D. Habs, and B. M. Hegelich, "Enhanced laser-driven ion acceleration in the relativistic transparency regime," Phys. Rev. Lett. **103**, 045002 (2009).
[32]J. H. Bin, W. J. Ma, H. Y. Wang, M. J. V. Streeter, C. Kreuzer, D. Kiefer, M. Yeung, S. Cousens, P. S. Foster, B. Dromey, X. Q. Yan, R. Ramis, J. Meyer-ter Vehn, M. Zepf, and J. Schreiber, "Ion acceleration using relativistic pulse shaping in near-critical-density plasmas," Phys. Rev. Lett. **115**, 064801 (2015).
[33]H. W. Powell, M. King, R. J. Gray, D. A. MacLellan, B. Gonzalez-Izquierdo, L. C. Stockhausen, G. Hicks, N. P. Dover, D. R. Rusby, D. C. Carroll, H. Padda, R. Torres, S. Kar, R. J. Clarke, I. O. Musgrave, Z. Najmudin, M. Borghesi, D. Neely, and P. McKenna, "Proton acceleration enhanced by a plasma jet in expanding foils undergoing relativistic transparency," New Journal of Physics **17**, 103033 (2015).
[34]Y. T. Li, J. Zhang, L. M. Chen, Y. F. Mu, T. J. Liang, Z. Y. Wei, Q. L. Dong, Z. L. Chen, H. Teng, S. T. Chun-Yu, W. M. Jiang, Z. J. Zheng, and X. W. Tang, "Hot electrons in the interaction of femtosecond laser pulses with foil targets at a moderate laser intensity," Phys. Rev. E **64**, 046407 (2001).
[35]D. F. Cai, Y. Q. Gu, Z. J. Zheng, W. M. Zhou, X. D. Yang, C. Y. Jiao, H. Chen, T. S. Wen, and S. T. Chunyu, "Double-peak emission of hot electrons generated by femtosecond laser interaction with solid targets," Phys. Rev. E **70**, 066410 (2004).
[36]G. Malka and J. L. Miquel, "Experimental confirmation of ponderomotive-force electrons produced by an ultrarelativistic laser pulse on a solid target," Phys. Rev. Lett. **77**, 75–78 (1996).
[37]J. Zhang, J. Zhang, Z. M. Sheng, Y. T. Li, Y. Qiu, Z. Jin, and H. Teng, "Emission direction of fast electrons in laser-solid interactions at intensities from the nonrelativistic to the relativistic," Phys. Rev. E **69**, 046408 (2004).
[38]R. Tommasini, E. Fill, R. Bruch, and G. Pretzler, "Generation of monoenergetic ultrashort electron pulses from a fs laser plasma," Applied Physics B **79**, 923–926 (2004).
[39]S. Feister, D. R. Austin, J. T. Morrison, K. D. Frische, C. Orban, G. Ngirmang, A. Handler, J. R. H. Smith, M. Schillaci, J. A. LaVerne, E. A. Chowdhury, R. R. Freeman, and W. M. Roquemore, "Relativistic electron acceleration by mj-class khz lasers normally incident on liquid targets," Opt. Express **25**, 18736–18750 (2017).
[40]Y. T. Li, X. H. Yuan, M. H. Xu, Z. Y. Zheng, Z. M. Sheng, M. Chen, Y. Y. Ma, W. X. Liang, Q. Z. Yu, Y. Zhang, F. Liu, Z. H. Wang, Z. Y. Wei, W. Zhao, Z. Jin, and J. Zhang, "Observation of a fast electron beam emitted along the surface of a target irradiated by intense femtosecond laser pulses," Phys. Rev. Lett. **96**, 165003 (2006).
[41]T. Toncian, C. Wang, E. McCary, A. Meadows, A. Arefiev, J. Blakeney, K. Serratto, D. Kuk, C. Chester, R. Roycroft, L. Gao, H. Fu, X. Yan, J. Schreiber, I. Pomerantz, A. Bernstein, H. Quevedo, G. Dyer, T. Ditmire, and B. Hegelich, "Non-maxwellian electron distributions resulting from direct laser acceleration in near-critical plasmas," Matter and Radiation at Extremes **1**, 82 – 87 (2016).
[42]Y. Ma, J. Zhao, Y. Li, D. Li, L. Chen, J. Liu, S. J. D. Dann, Y. Ma, X. Yang, Z. Ge, Z. Sheng, and J. Zhang, "Ultrahigh-charge electron beams from laser-irradiated solid surface," Proceedings of the National Academy of Sciences (2018), 10.1073/pnas.1800668115, http://www.pnas.org/content/early/2018/06/13/1800668115.full.pdf.
[43]J. Y. Mao, L. M. Chen, K. Huang, Y. Ma, J. R. Zhao, D. Z. Li, W. C. Yan, J. L. Ma, M. Aeschlimann, Z. Y. Wei, and J. Zhang, "Highly collimated monoenergetic target-surface electron acceleration in near-critical-density plasmas," Applied Physics Letters **106**, 131105 (2015), https://doi.org/10.1063/1.4916636.
[44]A. Jullien, A. Ricci, F. Böhle, J.-P. Rousseau, S. Grabielle, N. Forget, H. Jacqmin, B. Mercier, and R. Lopez-Martens, "Carrier-envelope-phase stable, high-contrast, double chirped-pulse-amplification laser system," Opt. Lett. **39**, 3774–3777 (2014).
[45]F. Böhle, M. Kretschmar, A. Jullien, M. Kovacs, M. Miranda, R. Romero, H. Crespo, U. Morgner, P. Simon, R. Lopez-Martens, and T. Nagy, "Compression of cep-stable multi-mj laser pulses down to 4 fs in long hollow fibers," Laser Physics Letters **11**, 095401 (2014).
[46]M. Ouillé, F. Böhle, A. Vernier, M. Bocoum, A. Jullien, M. Lozano, J-P. Rousseau, D. Gustas, D. Guénot, M. Kovacs, A. Blumenstein, P. Simon, J. Faure, S. Haessler, T. Nagy, and R. Lopez-Martens, "Relativistic-intensity near-single-cycle pulses at 1 kHz," (unpublished).
[47]M. Bocoum, F. Böhle, A. Vernier, A. Jullien, J. Faure, and R. Lopez-Martens, "Spatial-domain interferometer for measuring plasma mirror expansion," Optics Letters **40**, 3009–3012 (2015).
[48]`http://warp.lbl.gov`
[49]J.-L. Vay, D. P. Grote, R. H. Cohen, and A. Friedman, "Novel methods in the particle-in-cell accelerator code-framework warp," Computational Science & Discovery **5**, 014019 (2012).
[50]`https://www.picsar.net`
[51]H. Vincenti and J.-L. Vay, "Detailed analysis of the effects of stencil spatial variations with arbitrary high-order finite-difference maxwell solver," Computer Physics Communications **200**, 147 – 167 (2016).
[52]H. Vincenti, M. Lobet, R. Lehe, R. Sasanka, and J.-L. Vay, "An efficient and portable simd algorithm for charge/current deposition in particle-in-cell codes," Computer Physics Communications **210**, 145 – 154 (2017).
[53]H. Vincenti and J.-L. Vay, "Ultrahigh-order maxwell solver with extreme scalability for electromagnetic pic simulations of plasmas," Computer Physics Communications **228**, 22 – 29 (2018).
[54]P. Gibbon, *Short pulse laser interactions with matter* (World Scientific Publishing Company, 2004).
[55]J. P. Colombier, P. Combis, A. Rosenfeld, I. V. Hertel, E. Audouard, and R. Stoian, "Optimized energy coupling at ultrafast laser-irradiated metal surfaces by tailoring intensity envelopes: Consequences for material removal from al samples," Phys. Rev. B **74**, 224106 (2006).
[56]W. L. Kruer, *The physics of laser plasma interactions* (Addison-Wesley, New-York, 1988).

[57] C. McGuffey, A. G. R. Thomas, W. Schumaker, T. Matsuoka, V. Chvykov, F. J. Dollar, G. Kalintchenko, V. Yanovsky, A. Maksimchuk, K. Krushelnick, V. Y. Bychenkov, I. V. Glazyrin, and A. V. Karpeev, "Ionization induced trapping in a laser wakefield accelerator," Phys. Rev. Lett. **104**, 025004 (2010).

[58] A. Pak, K. A. Marsh, S. F. Martins, W. Lu, W. B. Mori, and C. Joshi, "Injection and trapping of tunnel-ionized electrons into laser-produced wakes," Phys. Rev. Lett. **104**, 025003 (2010).